X-Ray Variability in the Young Massive Triple #2 Orionis A

The Astrophysical Journal, 653:636–646, 2006 December 10

X-RAY VARIABILITY IN THE YOUNG MASSIVE TRIPLE θ^2 ORIONIS A

Norbert S. Schulz,[1] Paola Testa,[1] David P. Huenemoerder,[1]
Kazunori Ishibashi,[1] and Claude R. Canizares[1]
Received 2006 July 3; accepted 2006 August 18

ABSTRACT

Massive stars rarely show intrinsic X-ray variability. One exception is θ^2 Ori A, which has shown strong variability over the last 5 years. We observed a large outburst of the X-ray source with the High Energy Transmission Grating Spectrometer on board *Chandra* and compare the emissivity and line properties in states of low and high flux. The low state indicates temperatures well above 25 MK. In the high state we find high emissivities in the range from 3 to over 100 MK. The outburst event in stellar terms is one of the most powerful ever observed and the most energetic one in the ONC, with a lower total energy limit of 1.5×10^{37} ergs. The line diagnostics indicate that the line-emitting regions in the low states are as close as within 1–2 stellar radii from the O star's photosphere, whereas the hard states suggest a distance of 3–5 stellar radii. We discuss the results in the context of stellar flares, magnetic confinement, and binary interactions. By matching the dates of all observations with the orbital phases of the spectroscopy binary orbit, we find that outbursts occur very close to the periastron passage of the stars. We argue that the high X-ray states are possibly the result of reconnection events from magnetic interactions of the primary and secondary stars of the spectroscopic binary. Effects from wind collisions seem unlikely for this system. The line properties in the low state seem consistent with some form of magnetic confinement. We also detect Fe fluorescence indicative of the existence of substantial amounts of neutral Fe in the vicinity of the X-ray emission.

Subject headings: binaries: general — plasmas — stars: early-type — techniques: spectroscopic — X-rays: stars

Online material: color figures

1. INTRODUCTION

The number of massive stars in the Orion Nebula Cluster (ONC) is small compared to other young star clusters of its class, but the few it harbors have gained much attention in recent years. At the forefront are the members of the Orion Trapezium, specifically the peculiar O5.5 V star θ^1 Ori C (Schulz et al. 2001; Gagné et al. 2005a, 2005b), which have been under some scrutiny lately for their peculiar X-ray behavior (Schulz et al. 2003; Stelzer et al. 2005). Most of the massive stars in the ONC show magnetic properties of some form, either intrinsically or due to an unseen T Tauri companion. With respect to intrinsic magnetic peculiarity there are so far three massive OB stars with direct evidence of a sizable magnetic field: θ^1 Ori C, HD 191612, and τ Sco (Donati et al. 2002, 2006a, 2006b). Other massive Trapezium stars exhibit similar X-ray spectral properties to θ^1 Ori C, although in none of these stars has a magnetic field been directly measured, nor has any type of X-ray variability been reported until recently (Feigelson et al. 2002; Stelzer et al. 2005). Possible magnetic properties of some sort of fossil origin have been suggested for most of them (Schulz et al. 2001, 2003).

The primary star in θ^2 Ori A is the second most massive early-type star in the ONC after θ^1 Ori C. It is part of a massive system that had its share of mystery in the early days of X-ray astronomy, when some studies proposed to identify the star as the optical counterpart of the X-ray source 2U 0526−06 (Barbon et al. 1972; Aikman & Goldberg 1974) and later of 4U 0531−05 (Bernacca & Bianchi 1979). One of the main properties that made it a good candidate was its high-mass function. Its massive primary, a 5th magnitude O9.5 V star (Abt et al. 1991) of 25 $M_\odot$ (Preibisch et al. 1999), indicated the existence of one or more massive companions. Specifically, the lack of spectral signatures from a companion star at the time hinted the possibility of the existence of a compact object. Today it is recognized that the system is unlikely to harbor a compact star but is considered to be at least a massive triple system containing a visual companion with a mass of $<8\,M_\odot$ separated by $\sim 0\farcs4$ (Preibisch et al. 1999) and a spectroscopic companion to the primary with a mass of likely <7–$9\,M_\odot$ (Abt et al. 1991). The stellar types of both companion stars are still highly uncertain and range from a massive early A-type star for the visual companion to a B-type star as early as about B5 for the spectroscopic companion. Also notable is the physical closeness of these massive companions, which amounts for the visual companion to be 174 AU and the spectroscopic companion to be 0.47 AU (Preibisch et al. 1999), approximately 10 stellar radii off the primary. The system is likely as young as θ^1 Ori C, i.e., $\sim$0.3 Myr, which is also reflected in the fact that the orbital motion of the spectroscopic binary and the O star's rotational period are not yet synchronized. It cannot be much younger, as it already arrived on the zero-age main sequence, but also not much older through its association with the Orion Trapezium.

In a recent study of X-ray-emitting young stars in the Orion Nebula, Feigelson et al. (2002) found that θ^2 Ori A and several early B stars show short-timescale variability. Especially, θ^2 Ori A exhibited the most dramatic X-ray variability with a 50% flux drop over a time period of 10 hr superimposed by multiple small flares with a few hour durations. Until today this kind of variability in a massive system stands out as the most dramatic ever observed. The *Chandra* Orion Ultradeep Project (COUP) observations (Getman et al. 2005) a few years later covered the X-ray intensity of that star in several episodes for over 13 days and found it only weakly variable with the largest variation around a factor of 1.8 (Stelzer et al. 2005). The observed variability in θ^2 Ori A clearly represents problems not only with the standard model of wind shocks in massive stars, but also with the proposed model of

[1] Kavli Institute for Astrophysics and Space Research, Massachusetts Institute of Technology, Cambridge, MA 02139.

TABLE 1
ALL *Chandra* OBSERVATIONS THAT INCLUDE θ^2 ORI A

Observation ID	Start Date (UT)	Start Time (UT)	Exposure (ks)	Instrument	HETG First-Order Rate (10^{-2} counts s^{-1})	Phase Range
0018	1999 Oct 12	10:19:12	45.3	ACIS-I	...	0.86–0.89
0003	1999 Oct 31	05:47:21	52.0	HETGS	1.48	0.76–0.79
0004	1999 Nov 24	12:37:54	33.8	HETGS	3.91	0.92–0.99
1522	2000 Apr 1	17:31:12	37.5	ACIS-I	...	0.08–0.10
2567	2001 Dec 28	12:25:56	46.4	HETGS	3.92	0.99–1.01
2568	2002 Feb 19	20:29:42	46.3	HETGS	3.23	0.53–0.55
4395	2003 Jan 8	20:58:19	100.0	ACIS-I	...	0.33–0.38
3744	2003 Jan 10	16:17:39	164.2	ACIS-I	...	0.42–0.51
4373	2003 Jan 13	07:34:44	171.5	ACIS-I	...	0.54–0.64
4374	2003 Jan 16	00:00:38	169.0	ACIS-I	...	0.67–0.77
4396	2003 Jan 18	14:34:49	164.6	ACIS-I	...	0.79–0.88
3498	2003 Jan 21	06:10:28	69.0	ACIS-I	...	0.93–0.96
4473	2004 Nov 3	01:48:04	49.8	HETGS	2.80	1.00–1.03
4474	2004 Nov 23	07:48:38	51.2	HETGS	19.31	0.96–0.99

magnetically confined winds in these stars (Gagné et al. 2005a, 2005b). Feigelson et al. (2002) acknowledged that in some occasions large excursions in flux can be created by occasional large shocks, as proposed by Feldmeier et al. (1997), but the temperature profile during these events as observed is not consistent with such predictions. In the case of θ^2 Ori A, a scenario was envisioned in which magnetic reconnection events near the stellar surface occur, which tentatively and qualitatively could explain the X-ray emission observed in the O9.7 Ib supergiant ζ Ori (Waldron & Cassinelli 2001). In this paper we present recent observations of θ^2 Ori A observed with the High Energy Transmission Grating Spectrometer (HETGS) on board *Chandra* in a low- and high-flux state.

2. OBSERVATIONS AND DATA REDUCTION

The massive star θ^2 Ori A was observed with the *Chandra* HETGS (Canizares et al. 2005) on several occasions between 1999 and 2005. Table 1 summarizes important observing parameters for all observations with *Chandra*. Fourteen observations amount to a total exposure of 1.2 Ms. All these observations provide at least a CCD quality X-ray spectrum with spectral resolving powers between 6 and 50. Six observations were performed using the HETGS to obtain highly resolved X-ray spectra with resolving powers between 180 and 1200. The observations performed during 1999 were also recorded at a different focal plane temperature, which before 2000 February was -110°C and -120°C afterward. This has some impact on the data reduction itself, as all data run through the same reduction pipeline but with less developed calibration products for the -110°C case. Some of the now commonly used corrections for CCD charge transfer inefficiency and gain would not be effective. The detected X-ray source in all of these observations was never farther away from the aim point than 3.′0, and less then 2.′2 for the grating observations. This is well within the margin where the grating line-spread functions do not suffer from a detectable degradation due to off-axis source position.

All observations were reprocessed using CIAO, version 3.2 with the most recent CIAO CALDB products. We used standard wavelength redistribution matrix files (RMFs) and generated ancillary response files (ARFs) using the provided aspect solutions.[2] Note that for the HETGS spectra the RMF is fairly independent of focal plane temperature; however, the order sorting has to be adjusted to the different pulse-height distributions of the CCD at -110°C. Here we simply followed the steps applied in the data reduction for the Trapezium stars described in Schulz et al. (2000). For all the HETGS observations we generated spectra and analysis products for the medium-energy gratings (MEG) +1 and -1 orders, as well as for the high-energy gratings (HEG) +1 and -1 orders. Table 1 shows that for all HETGS observations except ObsID 4474, the average count rate is similar and low. Therefore, for most parts of the analysis below we added all +1 and -1 orders of the MEG for ObsIDs 0003, 0004, 2567, 2568, and 4473. The same procedure was applied to the HEG spectra. ObsID 4474 offers much higher count rates, and we proceeded with separate HEG and MEG spectra.

Contamination of the spectra from source confusion is to a large part mitigated by the order sorting of the CCDs. The source itself is off the center of the Orion Trapezium Cluster, and its dispersed tracks do not interfere as much with cluster core stars as, for example, during the analysis of θ^1 Ori C (Schulz et al. 2000). In all the six HETGS data sets we only encountered a handful of doubtful emission lines, which all could be eliminated by the fact that they appeared only once in the HEG and MEG orders or were identified as a COUP source. The HETGS spectral analysis was performed with the Interactive Spectral Interpretation System (ISIS; Houck & Denicola 2000).

3. LONG-TERM VARIABILITY

Table 1 shows all *Chandra* observations of the resolved X-ray source. Unfortunately, the source is bright enough to cause severe pileup in the observations performed without the gratings. The piled rates range between 0.3 and 0.9 counts frame^{-1}, which is more than an order of magnitude above the pileup-free regime. This problem was already recognized by the previous studies, specifically for ObsID 1522, done in 2000 April (Feigelson et al. 2002), and the COUP observations from 2003 January (Stelzer et al. 2005). In order to mitigate the problem, these authors extracted a few percent of presumably unpiled flux from an annulus covering parts the outer, low count wings of the point-spread function. These results carry large uncertainties. We used the pileup model in ISIS (Davis 2001) and found that in the case of ObsID 1522 the flux is slightly underestimated, whereas in the COUP data the flux was likely up to 40% lower.

The observations carried out with the HETGS do not have the pileup problem in the dispersed spectra. Table 1 lists the integrated count rates for all first-order spectra. It is immediately recognized

[2] See http://asc.harvard.edu/ciao/threads/.

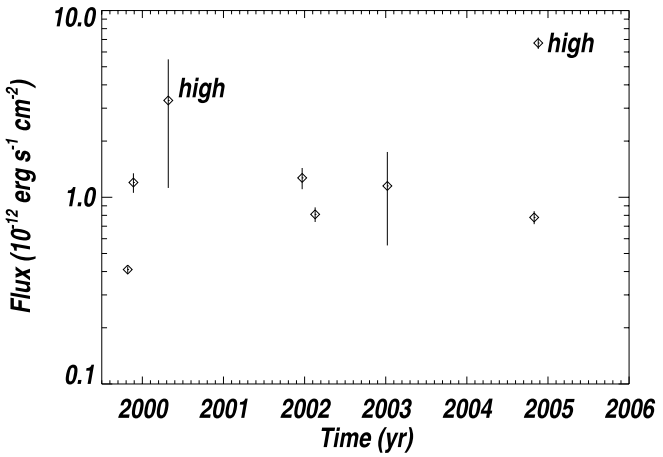

FIG. 1.—Light curve compiled from HETG first-order fluxes where available. For ObsID 1522 we used the estimates from Feigelson et al. (2002); for the COUP data we used the pileup model in ISIS (Davis 2001) to estimate the true count rate. The observations labeled high also exhibit extreme spectral hardening. Note that the value from the ObsID 1522 and COUP data has large systematic errors due to the effects of large pileup.

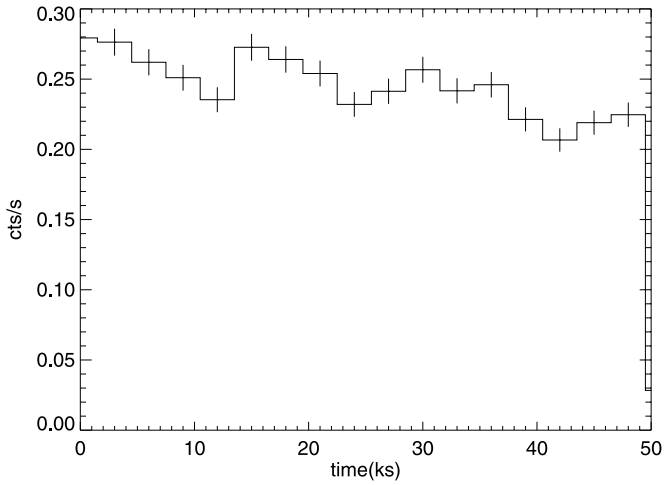

FIG. 3.—Light curve of the outburst in 2004 November (ObsID 4474). The data are in 3 ks bins and from the summed HETGS first orders. It shows about a 30% decline in flux with intermittent flaring. [*See the electronic edition of the Journal for a color version of this figure.*]

that there is a high level of variability in the source where the lowest and highest rate differ by a factor of 13. Specifically, the last observation stands out with an extreme rate. In an attempt to illustrate the long-term behavior of the source, we plotted the HETGS first-order fluxes together with the previously published estimates into a long-term light curve (see Fig. 1). For the HETGS spectra we simply apply the averaged flux from all integrated low-state grating spectra and scale it by the count rate from Table 1. We do this because the statistics of a dispersed spectrum from single low-state observations is insufficient. For ObsID 1522 we used a time-averaged flux from Feigelson et al. (2002). For the COUP data we also averaged the flux over the entire COUP exposure, even though the flux varied by almost a factor of 2 (Stelzer et al. 2005).

In Figure 1 we identify two high-flux and several lower flux states. The second "high" data point from 2004 clearly sticks out. The first data point marked as high from 2000 does not appear as extreme. However, its flarelike intrinsic light curve and its extreme hardness, which is very comparable to the high 2004 observation, indicates that the flux here is underestimated. The hardness in the COUP data, on the other hand, is very close to the one observed in the HETG low-flux observations. We therefore categorize the observation in ObsIDs 1522 and 4474 as "high state" and the others as "low state."

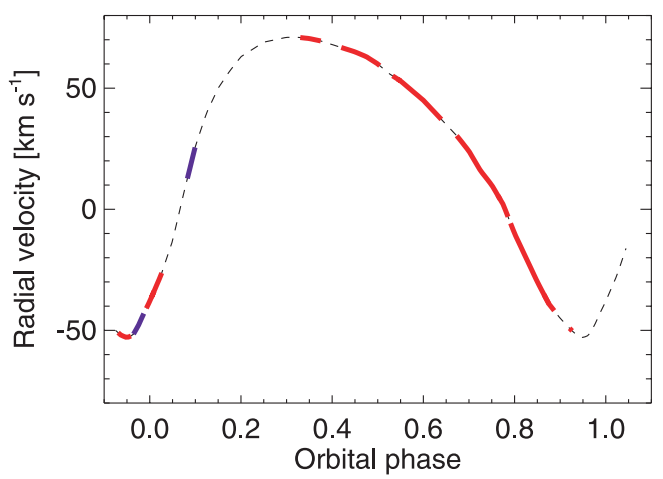

FIG. 2.—Phase coverage of all *Chandra* observations with the radial velocity curve of the secondary (Abt et al. 1991). The red colored phase ranges correspond to the low-state observations; the blue colors correspond to the high-state observations.

In order to further characterize the observed flux variability, we go one step farther and search for possible modulations of the observed X-ray with existing binary periods; θ^2 Ori A has a spectroscopic companion with a measured period of 20.974 days (Abt et al. 1991) and a projected distance of 0.47 AU (Preibisch et al. 1999). This distance is an average one, due to the determined orbital eccentricity of 0.33 and a large mass ratio of the two stars (Abt et al. 1991). We recognized that the two high states apparently seem to overlap within a similar phase of this orbital period. Figure 2 shows the measured radial velocity curve from Abt et al. (1991). It is highly asymmetric, with a rapid change in speed near periastron passage. The periastron passage has an ephemeris of HJD = 2,440,581.27 (Abt et al. 1991), from which we determined the orbital phase coverage of all the X-ray observations performed with *Chandra* so far.

The last column in Table 1 indicates the phase coverage for all the observations. Plotted in Figure 2, the red segments indicate observations, which we associated with the X-ray low state; the blue segments indicate high states. Strikingly visible is a close coincidence of the high-state emissivity with orbital periastron passage. It appears that the match is not perfect, i.e., the two high states appear right before and after phase 0 in a regime where the approach of the companion is closest, but low states have been detected in between these high states. Note that the light curve in Feigelson et al. (2002) indicates that the outburst started to wind down after orbital phase 0.08; thus, the onset likely happened around the phases 0.04–0.05. Figure 3 shows the light curve of the 2004 November outburst during orbital phase 0.96–0.99, where the X-ray flux stays nearly constant throughout the entire phase period. The flux appears to be persistently high, with a slow drop of about 30% from the start to the end. Future close tracking of the X-ray flux with orbital phase of the spectroscopic binary is clearly necessary.

4. ANALYSIS OF HETG SPECTRA

The analysis of the high-resolution X-ray spectra was performed for low- and high-state spectra. While we generally added positive and negative first orders for the MEG and HEG separately, we also

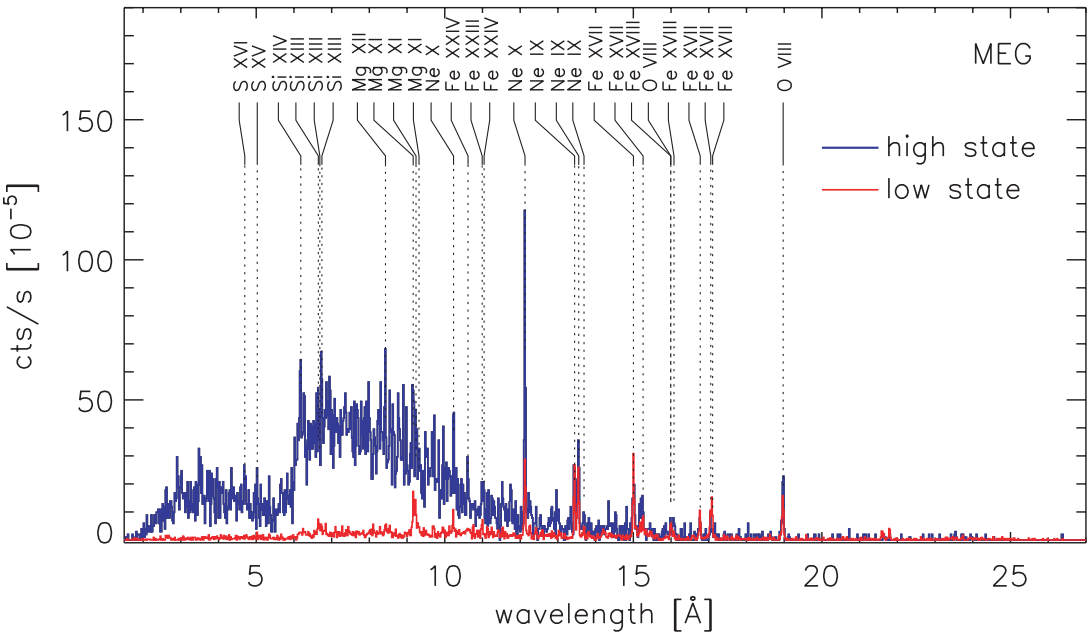

FIG. 4.—Summed HETG spectra (MEG only) for the low-state observations (*red*) and ObsID 4474 for the high-state observations (*blue*) with the identifications for the strongest lines. The spectra are binned to MEG resolution (0.01 Å).

treated the five low-state observations as one spectral state and added them together for statistical reasons. As can be seen in Table 1, the total number of counts in the high-state observation is still significantly higher than all low-state observations added together. The HETG spectra of the low state netted a total of 5807 counts and the high-state 9007 counts. These translate in observed (absorbed) fluxes of $(8.5 \pm 0.9) \times 10^{-13}$ ergs cm^{-2} s^{-1} in the low state and $(6.7 \pm 0.6) \times 10^{-12}$ ergs cm^{-2} s^{-1} for the high state in the 2–24 Å MEG band. The spectra are shown in Figure 4. Spectral diagnostics involves three parts. The first part is devoted to the detection and determination of the emission-line properties: i.e., line identifications, line positions, and line fluxes. The second part uses the line fluxes as well as underlying continuum to calculate corresponding emission measure distributions for the low and the high state. The third part then uses several emission lines and their ratios for to derive plasma parameters.

4.1. *Emission-Line Analysis*

We use the Astrophysical Plasma Emission Database (APED),[3] described by Smith et al. (2001) for the line identifications and line positions. We detected a total of 39 lines in the high state and 36 lines in the low state (Table 2). The line positions in all cases do not indicate significant shifts from the expected rest position. There is also no notable difference between the line position in the two states. The line fluxes were measured using custom software (PINTofALE; Kashyap & Drake 2000) and then corrected for the HETGS response. The Fe XXVI, Fe XXV, and Fe K line measurements are from HEG spectra; all the others are from MEG spectra.

The lines are generally unresolved and symmetric. In the regime of longer wavelengths, i.e., for lines from Fe XVII and Fe XVIII ions as well as O VIII, we observe some residual widths corresponding to about 300 km s^{-1}. The region around the Mg XI is heavily contaminated by various line blends from Fe and Ne ions. Here we only list the strongest candidates from Fe. For a more complete discussion, we refer to Testa et al. (2004). Table 2 also includes a line detection of neutral Fe K fluorescence at 1.93 Å during the high state. The line is detected close to the 2 σ level. Its line position and width limit the fluorescence emission to very low ionization levels between Fe I and Fe VII (House 1969).

[3] See http://hea-www.harvard.edu/APEC.

4.2. *Emission Measure Analysis*

The emission measure analysis was performed under the general assumption of collisional ionization equilibrium following Mazzotta et al. (1998) and abundances of Anders & Grevesse (1989). A general outline for the computation of the emission measure was given in Huenemoerder et al. (2001), which has now been successfully applied in several analyses of active coronal sources (Huenemoerder et al. 2003) and the hot star θ^1 Ori C (Schulz et al. 2003). The volume emission measure (VEM) specifies the X-ray emissivity within a specified volume. The differential emission measure (DEM) then is the VEM expressed as a function of temperature. We constructed this DEM from line fluxes listed in Table 2, spanning a range in log temperature of peak emissivity from 6.6 to 8.1. The method derives the emission measure and abundances simultaneously (Huenemoerder et al. 2003, 2006). We fit the high and low states separately. The range of uncertainties due to the data quality are given by the width of the curves in the figure, which was determined from Monte Carlo iteration. The lines used for the DEM calculation are marked in Table 2 for both states. Uncertainties due to atomic data are not included.

Lines were excluded from the fit if they were expected to be sensitive to density or photoexcitation (He-like triplet forbidden and intercombination lines), or if they had large residuals (possibly due to misidentification or blending). The normalization was adjusted post facto in order to set the line-to-continuum ratio, since the DEM solution was line-based. The result for both states is shown in Figure 5. The red curve is for the low state, and the blue curve is the high state. The thickness of the curves corresponds to the 68% confidence limits of the DEM. The filled areas cover the ranges of line temperature peak emissivities.

The low state continuously declines in emissivity above $\log T[\mathrm{K}] = 6.6$. The high state shows strong peaks at 7.1 and

TABLE 2
LINE IDENTIFICATIONS AND FLUXES IN THE LOW AND HIGH STATES

Ion	$\log T_{peak}$ (K)	λ_0 (Å)	λ_{low} (Å)	λ_{high} (Å)	Low-State Flux[a]	High-State Flux[a]
Fe XXVI[b]	8.1	1.780 (H)	...	1.766 ± 0.008	...	$9.0^{+8.0}_{-2.2}$
Fe XXV[b]	7.8	1.854 (L, H)	...	1.856 ± 0.005	...	$9.3^{+6.0}_{-2.8}$
Fe K	...	1.937	...	1.934 ± 0.004	...	$7.3^{+4.0}_{-2.3}$
S XVI[b]	7.4	4.729 (H)	...	4.725 ± 0.007	...	7.9 ± 2.2
S XV[b]	7.2	5.039 (L, H)	5.029 ± 0.008	5.030 ± 0.004	0.87 ± 0.58	12.2 ± 3.0
Si XIV[b]	7.2	6.182 (L, H)	6.182 ± 0.008	6.183 ± 0.003	0.54 ± 0.20	7.1 ± 1.7
Si XIV[c]	7.1	6.265	6.261 ± 0.008	6.279 ± 0.005	0.61 ± 0.21	5.9 ± 1.6
Si XIII[b]	7.0	6.648 (LH)	6.654 ± 0.006	6.651 ± 0.004	0.82 ± 0.24	4.1 ± 1.3
Si XIII	7.0	6.687	6.693 ± 0.018	6.688 ± 0.004	0.30 ± 0.20	3.1 ± 1.3
Si XIII	7.0	6.740	6.739 ± 0.018	6.741 ± 0.003	0.54 ± 0.22	5.5 ± 1.4
Fe XXIII	7.2	6.877	...	6.866 ± 0.004	...	3.5 ± 1.2
Fe XXIV	7.3	7.457	7.458 ± 0.015	...	0.35 ± 0.17	...
Mg XII[b]	7.0	8.421 (L)	8.427 ± 0.017	8.426 ± 0.002	0.28 ± 0.17	8.8 ± 1.6
Mg XII[c]	6.9	8.449	8.455 ± 0.010	...	0.53 ± 0.20	...
Fe XX[c]	7.1	9.143	9.141 ± 0.010	9.148 ± 0.005	0.41 ± 0.29	4.9 ± 2.4
Mg XI[b]	6.8	9.169 (H)	9.170 ± 0.003	9.167 ± 0.004	2.14 ± 0.47	5.6 ± 2.2
Fe XXI	7.1	9.194	9.208 ± 0.005	9.193 ± 0.004	1.21 ± 0.44	4.5 ± 2.2
Mg XI	6.8	9.231	9.239 ± 0.003	9.235 ± 0.004	2.28 ± 0.49	5.4 ± 1.7
Fe XX	7.0	9.282	9.287 ± 0.010	9.269 ± 0.005	0.83 ± 0.39	4.6 ± 1.9
Mg XI	6.8	9.314	9.315 ± 0.030	9.315 ± 0.007	0.57 ± 0.35	3.9 ± 1.9
Fe XX[c]	7.1	9.500	...	9.499 ± 0.005	...	4.7 ± 1.2
Ne X	6.8	9.708	...	9.723 ± 0.003	...	5.8 ± 1.7
Fe XX[c]	7.0	9.727	...	9.740 ± 0.007	...	2.8 ± 1.3
Ne X[b]	6.8	10.239 (L, H)	10.230 ± 0.004	10.238 ± 0.005	1.62 ± 0.36	5.5 ± 1.9
Fe XX[c]	7.0	10.252	...	10.252 ± 0.004	...	5.9 ± 1.9
Fe XXIV[b]	7.3	10.619 (H)	...	10.617 ± 0.005	...	5.9 ± 2.2
Fe XIX	6.9	10.645	...	10.638 ± 0.007	...	4.3 ± 2.0
Fe XXIV[b]	7.3	10.663 (H)	...	10.660 ± 0.007	...	2.3 ± 1.7
Fe XXIII[b]	7.2	10.981 (H)	...	10.993 ± 0.007	...	5.6 ± 2.4
Fe XXIV[b]	7.3	11.029 (H)	...	11.039 ± 0.009	...	5.2 ± 2.2
Ne X[b]	6.8	12.134 (L, H)	12.129 ± 0.002	12.134 ± 0.002	10.3 ± 1.9	56.8 ± 8.8
Fe XXIII	7.2	12.161	12.148 ± 0.004	...	3.8 ± 1.3	...
Fe XIX[b]	6.9	13.423 (L)	13.425 ± 0.002	...	0.57 ± 0.48	...
Ne IX[b]	6.6	13.447 (L, H)	13.448 ± 0.002	13.450 ± 0.005	13.6 ± 2.3	13.8 ± 6.6
Fe XIX	6.9	13.462	13.470 ± 0.002	...	2.6 ± 1.5	...
Fe XIX[b]	6.9	13.518 (L)	13.523 ± 0.002	...	4.4 ± 4.0	...
Ne IX	6.6	13.553	13.556 ± 0.002	13.557 ± 0.004	14.6 ± 2.0	22.8 ± 7.6
Fe XIX	6.9	13.645	13.647 ± 0.002	...	1.3 ± 0.9	...
Ne IX	6.6	13.699	13.702 ± 0.010	13.704 ± 0.010	2.8 ± 1.2	5.8 ± 4.9
Fe XVII[b]	6.7	15.014 (L, H)	15.014 ± 0.002	15.020 ± 0.004	30.2 ± 3.2	18.3 ± 9.2
Fe XIX	6.9	15.198	15.193 ± 0.007	15.210 ± 0.008	6.6 ± 2.1	12.0 ± 6.2
Fe XVII[b]	6.7	15.261 (L, H)	15.264 ± 0.004	15.269 ± 0.013	11.0 ± 2.6	12.1 ± 8.3
O VIII	6.5	16.006	16.008 ± 0.006	...	6.5 ± 2.2	...
Fe XVIII[b]	6.8	16.071 (L)	16.067 ± 0.009	...	2.9 ± 1.8	...
Fe XVII[b]	6.7	16.780 (L, H)	16.777 ± 0.004	16.768 ± 0.008	12.3 ± 2.9	14.5 ± 12.4
Fe XVII[b]	6.7	17.051 (L, H)	17.052 ± 0.004	17.050 ± 0.010	12.6 ± 2.7	12.4 ± 11.3
Fe XVII[b]	6.7	17.096 (L, H)	17.096 ± 0.003	17.100 ± 0.015	17.7 ± 3.5	7.7 ± 5.7
O VIII[b]	6.5	18.969 (L, H)	18.972 ± 0.004	18.984 ± 0.004	48.6 ± 8.3	71.0 ± 36.0
O VII	6.3	21.602	21.605 ± 0.008	...	15.6 ± 8.3	...
O VII	6.3	21.804	21.801 ± 0.005	...	23.0 ± 13.0	...

[a] In units of 10^{-6} photons cm^{-2} s^{-1}.
[b] Used for DEM solution: L = low state, H = high state; for Fe XXV, a lower flux limit was used in the low state.
[c] These identifications are either part of a blend or not unique due to temperature differences between low and high states.

7.9. We thus conclude, under the validity assumptions stated above, that the quality of the emission between the two states changes, and the difference is not solely due to the volume of emission.

Abundances, although uncertain (~20%–40%), for the derived DEM normalization were required to be about half-solar, except for Ne in the low state, which was near-solar. There is weak evidence that Fe and Ne were somewhat lower in the high state, with Fe changing from 0.65 to 0.15 and Ne from 1.0 to 0.5. The results represent mean values from the Monte Carlo iteration. The large range in the allowed emission measure couples to a range in abundance (but with strong correlations between different lines and temperatures). We do not find the abundance trends conclusive given the uncertainties present in the data and modeling, but they are suggestive of compositional changes in the plasma and warrant more careful examination. In θ^1 Ori C, abundances in the DEM

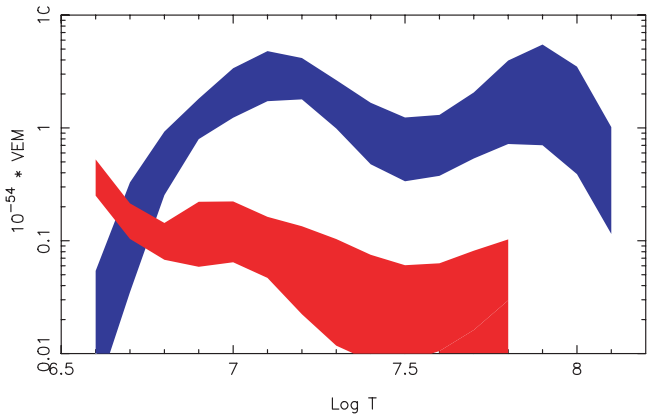

FIG. 5.—Emission measure distribution (in cubic centimeters) for the low (*red*) and the high (*blue*) state as calculated from the emission-line fluxes in Table 2. The upper and lower line boundaries are the 68% confidence limits.

suggested more nearly solar composition, but also showed a low Fe abundance (Schulz et al. 2003; Gagné et al. 2005a).

4.3. *Line Diagnostics*

Certain line ratios can be used to diagnose optical depth, densities, and sources of radiation. In the case of helium-like triplets it is the metastable forbidden line component that is sensitive to plasma density or, in the presence of radiation fields, to photoexcitation (Kahn et al. 2001; Blumenthal et al. 1972; Gabriel & Jordan 1969). We resolve the triplets in O VII, Ne IX, Mg XI, Si XIII, and S XV, although in the case of S XV, the range of sensitivity is quite limited (see Porquet et al. [2001] for an overview). We compute two ratios, an *R* ratio, which is the ratio between the forbidden and intercombination line flux, and the ratio of the H- to He-like resonance lines. While the former diagnoses plasma densities in the range between 10^{10} and 10^{15} cm^{-3} or a UV field between 900 and 1500 Å, the latter is sensitive to local plasma temperature. For the determination of these ratios, one has to be careful with the placement of the underlying continuum as well as interfering line blends. In nearly all cases the continua are strong and well determined (see Fig. 4), except for O VII in the high-state spectrum, which was too weak to be detected. Note that the temperature increase for the high state in the cool part of Figure 5 is shifted toward higher temperatures. In the low state it remains unclear where the cool temperature peak actually is. Interference by line blends is strong in Ne IX and Mg XI. For Ne IX Table 2 shows several known L-shell lines from Fe ions, which are well resolved and identified, but only for the low state. The Mg XI band has been modeled in detail by Ness et al. (2003). The Mg XI triplet, on the other hand, has interfering lines in both states. These are not identified and are likely satellite lines not included in APED. It should also be noted that, except for O VII, the forbidden lines are detected in all investigated ions.

The H- to He-like resonance line ratios and *R* ratios from the He-like triplets are summarized in Table 3. Interpretation of the *R* ratio requires additional information about the radiative environment. A sensitivity to density can only be claimed if sources of photoexcitation are ruled out or included in the calculation. On the other hand, if there are such sources, one may use the ratio to place limits to the distance from the radiation source to the line-forming region, as has been demonstrated for the hot star ζ Ori (Waldron & Cassinelli 2001). Under the assumption that the X-rays are produced in the O star wind, we calculated the dependence of the *R* ratio on the distance from the stellar photosphere. For this we assumed a stellar surface temperature of 30,000 K for the O9.5 star and used photoexcitation and decay rates from Blumenthal et al. (1972). Figure 6 then shows these functions for O VII, Ne IX, Mg XI, and Si XIII. The values of the *R* ratios are then plotted as diamonds onto these curves for the low state (*left*) and the high state (*right*). The 1 σ range for the ratios are highlighted as thick lines. It can be seen that the ratios of O VII and Si XIII are not well constrained. For Si XIII the range spreads over the entire sensitivity range of distance curve. In the case of O VII, the *R* ratio is in a range of the curve that is not very sensitive to distance. The deduced values place the ions within $\sim$5 stellar radii in both states. Ne IX and Mg XI are very well constrained. Ne IX shows no change between the high and low states. The range of radii for Mg XI seems to lie closer to the stellar surface in the low state. At these distances, the *R* ratio is always strongly affected by the O star's radiation field and is not a useful diagnostic of plasma density.

5. DISCUSSION

This study reveals several new aspects and details about the X-ray emission of young massive stars; θ^2 Ori A proves to be a new study case for variable emission from massive systems. The analysis confirms the findings by Feigelson et al. (2002) that this system undergoes strong excursions in X-ray flux. The outburst reported on in this study appears much more dramatic in terms of flux levels and spectral hardening even if one accounts for pileup, which heavily distorted the data in the 2000 event. Before we discuss the possible nature of the variable X-ray emission, we summarize the results of our analysis.

Over a period of about 5 years the X-ray source showed variability in flux of over an order of magnitude. During the last outburst the range of observed plasma temperatures changed from 3–30 MK to a range of from 3 to >100 MK. The X-ray luminosities changed from 2.6×10^{31} to 1.7×10^{32} ergs s^{-1}, which corresponds to a change of the L_X/L_{bol} ratio from $\sim 10^{-7}$ to $\sim 10^{-6}$. Under the assumption that all O stars are X-ray emitters of some form and the one in θ^2 Ori A is no exception, we have to assume that the radiation field of the primary O9.5 V star is the main source of destruction of the forbidden lines in the He-like triplets. The dominance of the UV field puts the X-ray source close, i.e., within a few stellar radii of the primary's photosphere. As a consequence, a possible contribution from high density to the

TABLE 3
H/He AND *R* RATIOS FOR THE LOW AND HIGH STATES

	Low State			High State		
Ion	Lyα/*r*	*T* (MK)	*f*/*i*	Lyα/*r*	*T* (MK)	*f*/*i*
O VII	3.1 ± 1.75	[2.2–4]	...	...	...	...
Ne IX	0.76 ± 0.19	[3.4–4.3]	0.20 ± 0.09	4.1 ± 2.0	[5, 4–10]	0.25 ± 0.20
Mg XI	0.13 ± 0.08	[3.7–5.2]	0.26 ± 0.15	1.6 ± 0.7	[7–16]	0.82 ± 0.53
Si XIII	0.66 ± 0.29	[8–13]	1.8 ± 1.4	1.7 ± 0.8	[8–18]	1.77 ± 0.83

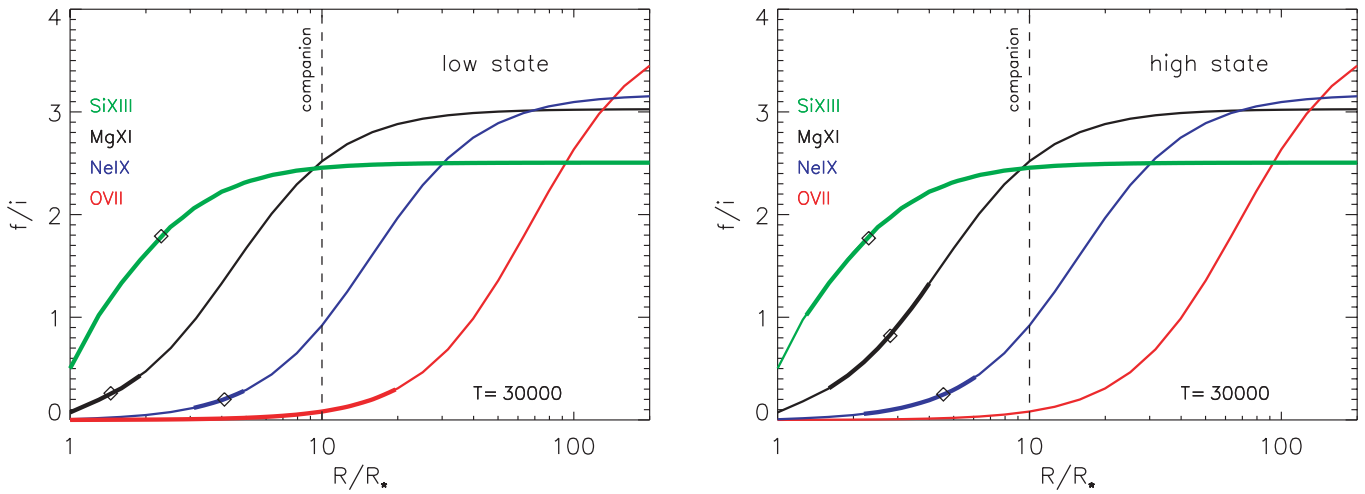

FIG. 6.—Dependence of the *R* ratios of the O VII, Ne IX, Mg XI, and Si XIII triplets on the distance to the stellar surface of the primary component in θ^2 Ori A for the low (*left*) and the high (*right*) state. The highlighted line portions represent the projected 1 σ confidence limits of the measured ratios. In the case of O VII there is only an upper limit in the low state. The surface temperature of the O9.5 star was assumed to be 30,000 K. The vertical hatched lines mark the distance of the spectroscopic companion as listed in Preibisch et al. (1999).

destruction of the lines is limited to the order of 10^{10} cm^{-3} for the low and high states at the most. High densities may only be feasible, if the X-ray source is at a very large distance from the O star and the entire emissivity is not associated with the O star wind. We are not discussing this possibility as consequently the O star itself would not be an X-ray emitter, which based on the observational record of X-rays from early-type stars is unlikely. The observed emissivities in these two states are then understood not only in terms of a change in the energy balance due to a dramatic change in temperatures, but also due to a vastly increased emissivity volume in the high state. Last but not least, the coincidence that the two outbursts appear close to the nearest approach of the spectroscopy companion suggests that they are related to some form of interaction.

In the following we discuss these results under various aspects. First we put the outbursts into the context of variability observed in the ONC so far with *Chandra*. We then attempt to qualitatively interpret the observed X-ray emissivity with respect to intrinsic physical environments such as magnetic confinement of winds, magnetic reconnection, and binary interactions. Last, we discuss possible origins of the Fe K fluorescence during the high state.

5.1. *Hard X-Ray Variability and Reconnection*

Figure 7 illustrates the extraordinary nature of the observed variability. We integrated the total energy of all bright flares of young late-type stars analyzed in Favata et al. (2005) in the COUP data and sorted them by flare energy. We integrated the flares from their observed maximum using the observed decay time. All the COUP flares have well-established peak luminosities, temperatures, and cooling time constants. The statistics then shows that most flares are found near a total energy of less than 10^{36} ergs, with the brightest one barely reaching 10^{37} ergs. In this respect the outburst in θ^2 Ori A from the year 2000 does not look particularly impressive with a total energy of 3×10^{36} ergs. However, the light curve in Feigelson et al. (2002) does not appear like the flares seen in late-type stars, which show a short rise and exponential decay. In both outbursts, however, the light curves showed their highest fluxes at the beginning of each observation with some form of decline afterward. Thus, we assumed the flux at the beginning of the light curve as the starting point and used the rest of the light curves to estimate its decay time. The integrated energy should then be considered a lower limit, because we do not really know the actual peak occurrence. The second outburst in 2004 in this respect clearly distinguishes itself from all the other observations as well as generic flares (see Fig. 3). The emissivity remains high over the entire exposure with some decline in flux. Under the assumption that the late 2004 event was some form of flare event, the resulting lower limit to the total energy is 1.5×10^{37} ergs.

Flares this powerful are unprecedented in normal stellar systems, and it is very likely that these high states are of a different origin. A somewhat less powerful flare has been recently uncovered in *Röntgensatellit* data of the massive binary σ Ori E (Groote & Schmitt 2004). For a flare event of coronal type the conditions have to be rather extreme indeed. Dissipation of large electrical currents associated with reconnection events realigning the field leads to the release of magnetic energy. Having established that the hard X-ray source during the outburst is likely located at a few stellar radii from the O star's surface, a corresponding magnetic

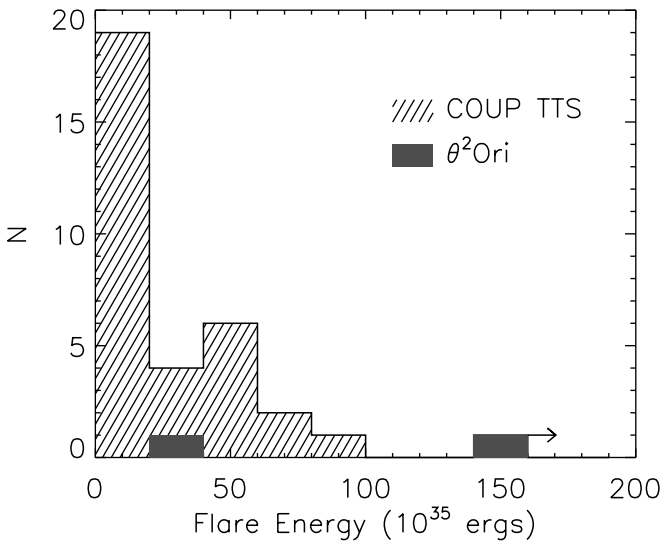

FIG. 7.—Number distribution of the integrated energy of all bright flares in the COUP study (Favata et al. 2005). [*See the electronic edition of the Journal for a color version of this figure.*]

loop structure seems extraordinarily large. Even though the star is expected to rotate relatively fast with rotation period between 2.8 days (Preibisch et al. 1999) and 3.5 days (Kaper 1999), the density of the wind at a few stellar radii is likely too low to cause the substantial field dragging necessary to explain the observed energy release. Such rotation rates produce surface velocities of about 1500 km s^{-1}, and we should have seen some line broadening from additional shocks or turbulence if the wind would be affected. Applying scaling laws of stellar flares from the Sun also show that reconnection events heat the ambient plasma on timescales of several minutes. Cooling times should be of order only a few hours. The outburst of 2004 persists for almost an entire day, suggesting that there is some continuous heating.

5.2. *Effects of Magnetic Confinement*

It is generally assumed that X-ray emission from hot stars originates from shocks in line-driven winds. O stars of all spectral and luminosity classes have so far been observed in X-rays. In hot stars such as θ^1 Ori C, τ Sco, and likely ζ Ori, energy is thought to be deposited into the wind through magnetic channeling resulting in hard X-ray emission. Since the main component of θ^2 Ori A is of O 9.5 V type, it seems warranted to associate at least some of the observed X-ray emission likely with the wind of the O star. It has also been recognized in recent years that temperatures much in excess of 15 MK cannot be the result of standard wind shocks, but are rather the result of more complex structures such as magnetic confinement or interacting winds.

In comparison with other hot stars (see Fig. 5 in Wojdowski & Schulz 2005) the DEMs of θ^2 Ori A show several novel aspects. Both the high and low states are different in their emissivity from what is expected from shocks in an unobstructed line-driven stellar wind. In the low state (*red curve*) the X-ray spectrum and its corresponding DEM compare well with X-ray emission from τ Sco, with the difference that we see not only strong emissivity at $\log T[\mathrm{K}] = 7$, but also emissivity at much lower temperatures. Unobstructed winds seem rather to peak below $\log T[\mathrm{K}] = 6.5$ with a steady decline of emissivity above about 3–5 MK. Two more facts strengthen the comparison with θ^1 Ori C and τ Sco: the emission lines are similarly narrow, and the origin of the emission is likely more than 1 stellar radius above the photosphere of the star. In both cases magnetic fields have been detected, most recently for τ Sco (Donati et al. 2006b). The emission from θ^2 Ori A in the low state then should be discussed in the context of some form of magnetic channeling of the O star wind.

In the high state the DEM of Figure 5 differs from anything we have observed before, i.e., a high emissivity from $\log T[\mathrm{K}] = 6.5$ to 8.0 with a tail toward even higher temperatures. Peak emissivities beyond $\log T[\mathrm{K}] = 7.5$ are known from flares in stars with active coronae and from θ^1 Ori C. The X-ray emissivity level in the latter star is an order of magnitude larger than observed at any level in θ^2 Ori A, owing to a stronger wind and a high magnetic field of order $\sim$1 kG (Gagné et al. 2005a). In θ^1 Ori C the soft emissivity is weak, and the bulk of the emissivity is growing toward higher temperatures. In θ^2 Ori A the outburst DEM rises high at lower temperatures and then remains high over a large range of high temperatures.

Since a magnetic field has not yet been directly measured in θ^2 Ori A, we rely on projections from the models presented by Babel & Montmerle (1997) and Gagné et al. (2005a) for the cases of IQ Aur and θ^1 Ori C. Clearly, the contrast between these two cases could not be larger, i.e., the mass-loss rates of a few times 10^{-10} and $10^{-7}\,M_\odot$ yr^{-1} differ by 3 orders of magnitude, and the surface temperatures (13,000 and 42,000 K, respectively) differ by over a factor of 3; θ^2 Ori A's values are somewhere in between. Mass-loss rates of less than $10^{-8}\,M_\odot$ yr^{-1} and a stellar surface temperature of 30,000 K suggest a strong wind. Under the assumption that the wind has a moderate velocity, i.e., v_∞ of order 1000 km s^{-1}, we would obtain a confinement parameter ($\eta = B^2R^2/\dot{M}v_\infty$) of 10 for the existence of a magnetic field of >0.6 kG.

Quantitative modeling by ud-Doula & Owocki (2002) suggests that a confinement parameter of 10 or above should result in effective confinement. The model also predicts that most X-rays are produced in a relatively small region where the density of the hot gas is high, beyond 10^{12} cm^{-3}. To reach such high densities and temperatures, confined regions form within 1 or 2 Alfvén radii from the stellar surface where field lines are still mostly closed and perpendicular to the magnetic equatorial plane. Thus, confinement places the X-ray source close to the stellar surface of the primary. For θ^2 Ori A, the R ratios in Figure 6 put the distance of the X-ray source less than 1 stellar radius in the case of Mg XI and 2–4 stellar radii in the case of Ne IX above the stellar surface. The confinement model and data in the case of θ^1 Ori C place the region of emission within $\sim$2 stellar radii (Gagné et al. 2005a).

Our data seem to rule out densities that are as high as 10^{12} cm^{-3}. However, the low-state spectrum indicates much lower emissivity at high temperatures than observed in θ^1 Ori C, suggesting that such high densities may not be required. The R ratios are not entirely conclusive with respect to the location of the emitting region above the stellar surface and predictions from magnetic confinement. In the low state, the Mg XI R ratio seems to indicate such a closeness; the Ne IX ratio, on the other hand, could allow for the larger range. In the high state the emission region is more like $3R_{\mathrm{star}}$–$5R_{\mathrm{star}}$ from the O star surface. Confinement in the latter case seems difficult to achieve. Thus, a simple confinement scenario, as proposed for θ^1 Ori C and likely τ Sco, is feasible for the low state but is problematic for the high state.

5.3. *Binary Interactions*

5.3.1. *Colliding Winds*

We also have to consider the fact that all stars in the θ^2 Ori A system are of early type, and thus, all are sources of radiatively driven winds. The proximity of the spectroscopic companion could then give rise to some form of wind interaction. Colliding wind scenarios to produce X-ray emission (Prilutskii & Usov 1976; Stevens et al. 1992) have been proposed since the launch of *Einstein*, where a survey of WR stars revealed that WR-O binary system are systematically brighter in X-rays (Pollock 1987). Recent observations of O star binaries such as HD 93403 (O5.5 I + O7 V; Rauw et al. 2002), HD 159176 (De Becker et al. 2004), and HD 152248 (O7 III + O7.5 III; Sana et al. 2004) involve O stars of very early type or luminosity classes III and above or both. Other cases involving O dwarfs and B stars such as HD 206267 and ι Ori have so far not been conclusive in X-rays (Pittard et al. 2000; Schulz 2003). Colliding wind scenarios are usually associated with exceptionally strong winds with mass-loss rates exceeding $10^{-6}\,M_\odot$ yr^{-1} and terminal velocities of >2000 km s^{-1}. Unusually bright X-rays from very young O star binaries have been observed in young star-forming regions containing many massive stars and in which strong stellar winds create a diffuse interstellar gas (Townsley et al. 2003).

The case of θ^2 Ori A is quite different. Its O9.5 V star may produce a mass loss of order only about $1 \times 10^{-8}\,M_\odot$ yr^{-1}. Its companion has likely a much lower rate. Recent research also suggests that mass-loss rates in Galactic O-type stars could be even smaller than generally assumed (Fullerton et al. 2006). A colliding wind scenario is expected to differ with respect to systems such as WR 140 or HD 152248, where mass-loss rates are over 1000 times

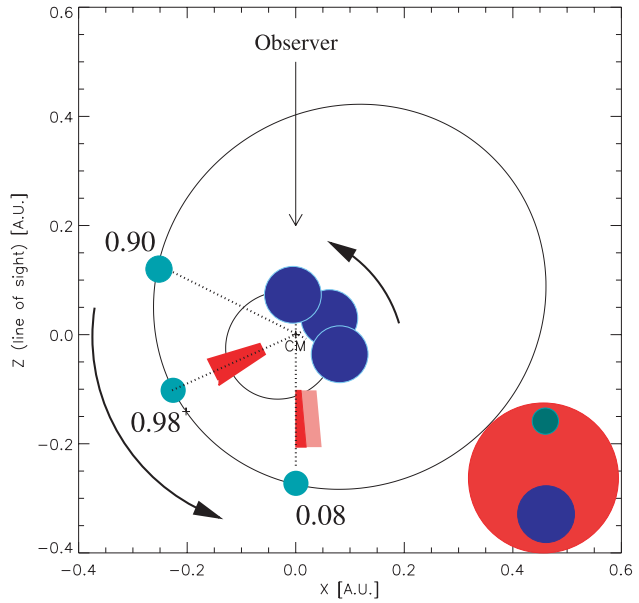

FIG. 8.—Schematic illustration of configurations of the binary using the orbital parameters given by Abt et al. (1991). The system is plotted face-on; the inclination toward the observer is estimated to be 65°. The black arrows indicate the direction of motion around the center of mass. The sizes of the stellar companions are scaled about proper to the orbit dimensions. The blue circle represents the O9.5 V star; the green circle represents the spectroscopic companion. The configuration at orbital phase 0.90 marks the projected start of outburst activity; the one at 0.98 marks the outburst observed in 2005 November; the one at 0.08 marks the start of the outburst reported by Feigelson et al. (2002) and the projected end of activity. We used the start of the flux decline in the light curve of the 2000 outburst to set the endpoint. Symmetrically to periastron we then projected the start point of the activity. The filled red areas mark the anticipated locations of the hard outburst X-ray emission. The lighter red shade indicates the decline of the 2000 outburst. The interaction region is large compared to the size of the primary star, and its moving through the line of sight should not affect the view of the X-ray source by much. This is visualized in the cartoon in lower right corner, which is now the line of sight view of the observer at 0.08 orbital phase.

higher. In HD 152248 the separation of the two stars is always close, within 2 primary stellar radii. Figure 8 shows that even at closest approach, the secondary in θ^2 Ori A is still over 6 primary radii apart from the O star surface, and wind densities should not exceed a few times 10^9 cm^{-3}. However, wind models also suggest that the density cannot be much lower either. At much lower densities heating is provided by collisionless shocks as in WR 140 (Pollock et al. 2005), but would require unrealistically high emission volumes on scales in excess of 6 AU. In the optimistic case of effective wind compression, which may allow for densities up to 10^{10} cm^{-3}, the volumes would be on the scale of only a few 0.01 AU. But then we still need an average collision speed $\gg$2000 km s^{-1} and near 100% collision efficiency, again extremely unrealistic conditions.

Furthermore, in colliding wind systems luminosity is inversely proportional to the distance from the companion to the shock interface, which at an orbital eccentricity of order 0.33, as suggested (Preibisch et al. 1999), would predict a slow and gradual increase and decrease over significant fractions of the binary orbit. The fact that we have low-state observations intermediate to the observed high states points to more explosive origins. We therefore rule out scenarios that involve interacting winds only.

5.3.2. *Interacting Magnetic Fields*

Section 5.1 already demonstrated that simple magnetic reconnection scenarios related to an O star's magnetic field alone seem unfeasible. On the other hand, the proximity of the outbursts to the periastron passage suggests the possibility of two-body magnetic interaction events. Figure 8 schematically illustrates the anticipated orbital geometry. In the two-body case, the X-ray source is located in between the two stars, which near periastron are separated by about 6–7 primary radii. With an integrated emissivity during the outburst of 2.1×10^{55} cm^{-3} the emitting volume has a size of (0.2 AU)^3, assuming realistic plasma densities. Magnetic reconnection thus has to happen on quite large scales. We can estimate an upper limit to the magnetic energy release by calculating the heat produced by the drag of the primary field lines due to the approaching companion to

$$\frac{dE_{\rm mag}}{dt} = \eta \Omega_{\rm rad} B_{\rm surf}^2 R_d^3, \qquad (1)$$

where $B_{\rm surf}$ is the field strength of the O star primary, $\Omega_{\rm rad}$ is the absolute difference between the angular velocity of the incoming secondary and the primary rotation, and R_d^3 is the size of the interaction region. The parameter η is an efficiency factor accounting for reconnection efficiency for specific geometries and accounting for the fact that not all magnetic field lines participate in a specific release event. A similar approach has been applied by Shu et al. (1997) to estimate the energy release in star-disk interactions in T Tauri stars. For a primary field of $\sim$0.6 kG and an incoming speed of the companion of 250 km s^{-1} we obtain a maximum energy release of $\sim 10^{36}$ ergs s^{-1}. This value should be compared to the observed luminosity during the outburst, which is a few times 10^{32} ergs s^{-1}. This indicates that η can be very small. It can also mean that our basic assumptions are incorrect. However, given the large emissivity volume and a likely weak companion field, this may not be unrealistic. Also, given the many unknowns in this system with respect to such a complex scenario, we cannot draw more detailed conclusions. More data and modeling clearly seem warranted.

5.4. *Origins of the* Fe *Fluorescence*

In the high state we also detect a few photons that we attribute to Fe K fluorescence at 1.93 Å. The outburst produces a substantial amount of X-ray continuum flux above 7.11 keV (1.74 Å), the value of the photoelectric absorption edge. Fluorescence emission emerges from cool, mostly neutral, and optically thick materials located near ionizing environments. In the X-ray band fluorescence is most efficient for Fe atoms because the high atomic number mitigates autoionization through Auger electrons. Fe fluorescence therefore has the highest yields, and strong Fe K lines are observed in X-ray binaries with large accretion disks (Gottwald et al. 1995), high column density material in winds (Sako et al. 1999; Schulz et al. 2002), and proto– and pre–main-sequence stellar disks (Tsujimoto et al. 2005), but also in the Sun (Bai 1979; Parmar et al. 1984).

The fact that we observe fluorescence in such a system is a novelty, if one disregards high-mass X-ray binaries, which also contain stars of early type with strong winds, but also neutron stars or stellar black holes. Here strong winds from evolved supergiants are almost completely ionized by a compact X-ray source giving rise to fluorescence emission from cool, optically thick clumps dispersed throughout the wind (Sako et al. 1999; Schulz et al. 2002; Boroson et al. 2003). Feldmeier (1995) pointed out that winds can have distinct regions of clumpy old materials, specifically in the outer regions of the wind. Recent work designed to explain the low attenuation of X-ray lines quite recently led to studies involving a general porosity of stellar winds (Owocki & Cohen 2006). Although the wind in the O9.5 dwarf may have

such clumpiness on some scale, we do not consider these as a possible source for the fluorescence because they do not provide a sufficient mass with respect to the incident luminosity. The X-ray source in Vela X-1 is of order 10^4 times brighter than the outburst in θ^2 Ori A.

We investigated a variety of possible sources and conclude that none of the sites alone can account for the observed photons. Young systems contain a lot of debris and circumstellar material even several million years after formation, and given the projected age of the system of less then 1 Myr, one should expect plenty of circumstellar matter in the system. However, the fact that the O star entered the main sequence also means that its powerful wind has evaporated most of circumstellar material within the spectroscopic binary with a probability of some leftover disk with the visual companion. This leaves us with the optically thick photospheres of the companion as well as any possible disk structure that evolved from the wind confinement.

In order to estimate the expectation of fluorescence from the O star's photosphere, we derived an efficiency for fluorescence from the stellar surface (Bai 1979) as $\epsilon \sim 2^* I_{\rm line}/I_c$, where I_c is the incident hard continuum flux above 7.11 keV and $I_{\rm line}$ is the measured fluorescence line flux. The model in Bai (1979) was designed to estimate photospheric fluorescence from the Sun, but since its geometry only scales with the stellar radius, we may relate the efficiency to the behavior in the Sun. For θ^2 Ori A we measured an efficiency $\epsilon = 0.064 \pm 0.045$. For the Sun $\epsilon = 0.04$ is expected at the surface and drops steeply above 1 solar radius (Parmar et al. 1984). Fluorescence from the photosphere alone is thus likely not sufficient to explain the observed line flux, which is consistent with the nondetection Fe fluorescence in θ^1 Ori C (Schulz et al. 2003), where the hard X-ray flux was even higher. This shows that the fluorescence has to include other sources mentioned above.

6. CONCLUSIONS

The X-ray emission from θ^2 Ori A showed unusually strong variability over the last 5 years. Its last outburst in 2004 November was energetically one of the most powerful recorded so far in a stellar system, consisting of only early-type stars. The outbursts appear to be near periastron passage, indicating a connection between a close approach of the companion and outburst activity.

The primary star is of O9.5 V type, and by its nature associated with a sizable radiatively driven wind. The fact that we observe narrow X-ray lines with maybe some turbulent broadening of $\sim$300 km s^{-1}, a hard emissivity distribution, and R ratios that indicate that the X-ray source is as close as <2 primary stellar radii to the O star's surface lets us conclude that the X-ray emission in the *low* state is enhanced by magnetic confinement of the wind possibly similar to the model that was successfully applied to θ^1 Ori C (Gagné et al. 2005a). We do not observe evidence for a hybrid behavior as in θ^1 Ori C (Schulz et al. 2003).

The X-ray lines in the *high* state appear mostly unresolved, again with some evidence of turbulent broadening in the soft lines. However, the emissivity distribution is now greatly enhanced at temperatures above 50 MK, and the R ratios indicate that the bulk of the X-ray emission arises from larger distance from the stellar surface. Based on our favored conclusion of a magnetic origin of the low-state emission and the association of the outbursts with a close approach of the massive spectroscopic binary star, we propose a scenario of intermittent, strong, and persistent reconnection events on likely various timescales as a consequence of interacting magnetic fields of the primary and secondary stars. Effects from wind collisions are not favored, mainly for reasons related the lack of sufficient wind density and the explosive appearance of the activity.

We also observe fluorescence emission for which we cannot assess a sufficiently potent candidate source. We therefore conclude that we observe a combination of many origins, such as the photospheres of the stars, confined wind disks, and some remnants from protostellar activity.

Support for this work was provided by the National Aeronautics and Space Administration (NASA) through the Smithsonian Astrophysical Observatory contract SV3-73016 to MIT for support of the *Chandra* X-Ray Center, which is operated by the Smithsonian Astrophysical Observatory for and on behalf of NASA under contract NAS 8-03060.

REFERENCES

Abt, H. A., Wang, R., & Cardona, O. 1991, ApJ, 367, 155
Aikman, G. C. L., & Goldberg, B. A. 1974, JRASC, 68, 205
Anders, E., & Grevesse, N. 1989, Geochim. Cosmochim. Acta, 53, 197
Babel, J., & Montmerle, T. 1997, A&A, 323, 121
Bai, T. 1979, Sol. Phys., 62, 113
Barbon, R., Bernacca, P. L., & Tarenghi, M. 1972, Nature, 240, 182
Bernacca, P. L., & Bianchi, L. 1979, A&A, 75, 61
Blumenthal, G. R., George, R., Drake, G. W. F., & Tucker, W. H. 1972, ApJ, 172, 205
Boroson, B., Vrtilek, S. D., Kallman, T., & Corcoran, M. 2003, ApJ, 592, 516
Canizares, C. R., et al. 2005, PASP, 117, 1144
Davis, J. E. 2001, ApJ, 562, 575
De Becker, M., Rauw, G., Pittard, J. M., Antokhin, I. I., Stevens, I. R., Gosset, E., & Owocki, S. P. 2004, A&A, 416, 221
Donati, J.-F., Babel, J., Harries, T. J., Howarth, I. D., Petit, P., & Semel, M. 2002, MNRAS, 333, 55
Donati, J.-F., Howarth, I. D., Bouret, J.-C., Petit, P., Catala, C., & Landstreet, J. 2006a, MNRAS, 365, L6
Donati, J.-F., et al. 2006b, MNRAS, 370, 629
Favata, F., Flaccomio, E., Reale, F., Micela, G., Sciortino, S., Shang, H., Stassun, K. G., & Feigelson, E. D. 2005, ApJS, 160, 469
Feigelson, E. D., Broos, P., Gaffney, J. A., III, Garmire, G., Hillenbrand, L. A., Pravdo, S. H., Townsley, L., & Tsuboi, Y. 2002, ApJ, 574, 258
Feldmeier, A. 1995, A&A, 299, 523
Feldmeier, A., Puls, J., & Pauldrach, A. W. 1997, A&A, 322, 878
Fullerton, A. W., Massa, D. L., & Prinja, R. K. 2006, ApJ, 637, 1025
Gabriel, A. H., & Jordan, C. 1969, MNRAS, 145, 241
Gagné, M., Oksala, M. E., Cohen, D. H., Tonnesen, S. K., ud-Doula, A., Owocki, S. P., Townsend, R. H. D., & MacFarlane, J. J. 2005a, ApJ, 628, 986
———. 2005b, ApJ, 634, 712
Getman, K. V., et al. 2005, ApJS, 160, 319
Gottwald, M., Parmar, A. N., Reynolds, A. P., White, N. E., Peacock, A., & Taylor, B. G. 1995, A&AS, 109, 9
Groote, D., & Schmitt, J. H. M. M. 2004, A&A, 418, 235
Houck, J. C., & Denicola, L. A. 2000, in ASP Conf. Ser. 216, Astronomical Data Analysis Software and Systems IX, ed. N. Manset, C. Veillet, & D. Crabtree (San Francisco: ASP), 591
House, L. L. 1969, ApJS, 18, 21
Huenemoerder, D. P., Canizares, C. R., Drake, J. J., & Sanz-Forcada, J. 2003, ApJ, 595, 1131
Huenemoerder, D., Canizares, C. R., & Schulz, N. S. 2001, ApJ, 559, 1135
Huenemoerder, D. P., Testa, P., & Buzasi, D. 2006, ApJ, 650, 1119
Kahn, S. M., Leutenegger, M. A., Cottam, J., Rauw, G., Vreux, J.-M., den Boggende, A. J. F., Mewe, R., & Güdel, M. 2001, A&A, 365, L312
Kaper, L. 1999, in IAU Colloq. 169, Variable and Non-spherical Stellar Winds in Luminous Hot Stars, ed. B. Wolf, O. Stahl, & A. W. Fullerton (Berlin: Springer), 193
Kashyap, V., & Drake, J. J. 2000, Bull. Astron. Soc. India, 28, 475
Mazzotta, P., Mazzitelli, G., Colafrancesco, S., & Vittorio, N. 1998, A&AS, 133, 403
Ness, J.-U., Brickhouse, N. S., Drake, J. J., & Huenemoerder, D. P. 2003, ApJ, 598, 1277
Owocki, S. P., & Cohen, D. 2006, ApJ, 648, 565

Parmar, A. N., Culhane, J. L., Rapley, C. G., Wolfson, C. J., Acton, L. W., Phillips, K. J. H., & Dennis, B. R. 1984, ApJ, 279, 866
Pittard, J. M., Stevens, I. R., Corcoran, M. F., Gayley, K. G., Marchenko, S. V., & Rauw, G. 2000, MNRAS, 319, 137
Pollock, A. M. T. 1987, ApJ, 320, 283
Pollock, A. M. T., Corcoran, M. F., Stevens, I. R., & Williams, P. M. 2005, ApJ, 629, 482
Porquet, D., Mewe, R., Dubau, J., Raassen, A. J. J., & Kaastra, J. S. 2001, A&A, 376, 1113
Preibisch, T., Balega, Y., Hoffmann, K.-H., Weigelt, G., & Zinnecker, H. 1999, NewA, 4, 531
Prilutskii, O. F., & Usov, V. V. 1976, AZh, 53, 6
Rauw, G., Vreux, J.-M., Stevens, I. R., Gosset, E., Sana, H., Jamar, C., & Mason, K. O. 2002, A&A, 388, 552
Sako, M., Liedahl, D. A., Kahn, S. M., & Paerels, F. 1999, ApJ, 525, 921
Sana, H., Stevens, I. R., Gosset, E., Rauw, G., & Vreux, J.-M. 2004, MNRAS, 350, 809
Schulz, N. S. 2003, Rev. Mex. AA Ser. Conf., 15, 220
Schulz, N. S., Canizares, C., Huenemoerder, D., Kastner, J. H., Taylor, S. C., & Bergstrom, E. J. 2001, ApJ, 549, 441
Schulz, N. S., Canizares, C., Huenemoerder, D., & Lee, J. 2000, ApJ, 545, L135
Schulz, N. S., Canizares, C., Huenemoerder, D., & Tibbets, K. 2003, ApJ, 595, 365
Schulz, N. S., Canizares, C. R., Lee, J. C., & Sako, M. 2002, ApJ, 564, L21
Shu, F. H., Shang, H., Glassgold, A. E., & Lee, T. 1997, Science, 277, 1475
Smith, R. K., Brickhouse, N. S., Liedahl, D. A., & Raymond, J. C. 2001, ApJ, 556, L91
Stelzer, B., Flaccomio, E., Montmerle, T., Micela, G., Sciortino, S., Favata, F., Preibisch, T., & Feigelson, E. D. 2005, ApJS, 160, 557
Stevens, I. R., Blondin, J. M., & Pollock, A. M. T. 1992, ApJ, 386, 265
Testa, P., Drake, J. J., & Peres, G. 2004, ApJ, 617, 508
Townsley, L. K., Feigelson, E. D., Montmerle, T., Broos, P. S., Chu, Y.-H., & Garmire, G. P. 2003, ApJ, 593, 874
Tsujimoto, M., Feigelson, E. D., Grosso, N., Micela, G., Tsuboi, Y., Favata, F., Shang, H., & Kastner, J. H. 2005, ApJS, 160, 503
ud-Doula, A., & Owocki, S. P. 2002, ApJ, 576, 413
Waldron, W. L., & Cassinelli, J. P. 2001, ApJ, 548, L45
Wojdowski, P. S., & Schulz, N. S. 2005, ApJ, 627, 953